Generation of Human Walking Paths

Alessandro Vittorio Papadopoulos · **Luca Bascetta** · **Gianni Ferretti**

Abstract This work investigates the way humans plan their paths in a goal-directed motion, assuming that a person acts as an optimal controller that plans the path minimizing a certain (unknown) cost function. Taking this viewpoint, the problem can be formulated as an inverse optimal control one, i.e., starting from control and state trajectories one wants to figure out the cost function used by a person while planning the path. The so-obtained model can be used to support the design of safe human-robot interaction systems, as well as to plan human-like paths for humanoid robots. To test the envisaged ideas, a set of walking paths of different volunteers were recorded using a motion capture facility. The collected data were used to compare two solutions to the inverse optimal control problem coming from the literature to a novel one. The obtained results, ranked using the discrete Fréchet distance, show the effectiveness of the proposed approach.

A.V. Papadopoulos
Department of Automatic Control, Lund University, Lund, Sweden
Tel.: +46-46-2228777
Fax: +46-46-138118
E-mail: alessandro.papadopoulos@control.lth.se

L. Bascetta, and G. Ferretti
Dipartimento di Elettronica, Informazione e Bioingegneria, Politecnico di Milano, Milano, Italy

1 Introduction

In the last decade there was an increasing interest of robotic researchers towards robot co-workers and human-robot co-existence and cooperation [1,15,40,41,47]. These emerging research topics have shown their relevance either in the industrial robotics and in the service robotics scenarios.

In the former, the research aims at removing the fences between human workers and robots allowing for a fruitful co-operation, but keeping the interaction safe [8,36–38,47]. In this context, the knowledge of how a human plans a walking path is of utmost importance, as it allows to predict where a human is heading to, inferring a related danger level and triggering a suitable safety reaction. Improving the accuracy and reliability of the human walking model allows thus to increase the safety of the system and to reduce the conservatism of the safety controller.

In the latter, humanoid robots are getting closer to humans, helping impaired and elderly people in their everyday life duties, or receiving and guiding visitors in museums, exhibitions, and shopping malls [12]. In these contexts, predicting where a human is heading to, for example to give him the appropriate description of a picture or suitable advertisings related to a shop, is still an important issue. Nevertheless, developing a planner for humanoid robots in such a way that the planned paths are perceived by humans as human-like is even more important: increasing the human-likeliness of the path improves the social acceptance of such machines in everyday life.

The aforementioned motivations drove the research of the last decade on investigating how humans plan their walking paths. Researchers have been focused on the study of the so-called goal-oriented motion model [3, 5, 16, 30, 33], i.e., where the humans walk from an initial pose towards a predefined goal pose, assuming that the process adopted by humans to plan their walking paths can be represented as the

solution of an optimal control problem. Adopting this framework, the problem can be converted into the investigation of the cost function the human is supposed to minimize.

The same framework is addressed in this paper and can be formulated in more detail as follows: given a set of experimentally recorded goal-directed walking paths, select a motion model and a cost function in such a way that the paths generated as solutions of the optimal control problems (whose dynamic constraints and optimality criteria are the aforementioned motion model and cost function), each one having as initial and final conditions the human pose at the first and last point of the experimental path, resemble as much as possible the corresponding experimental ones.

In this paper we extend the work in [32], presenting a novel cost function that considers the normalized energy and position of the human with respect to the target. The results obtained with this cost function are compared to others presented in the literature, adopting the discrete Fréchet distance [2] as a metric to assess the similarity of a set of paths, as opposite to standard approaches that use the Euclidean one, e.g., [5, 22, 34]. The overall objective of this work is not just to identify a motion model and a cost function that can suitably interpolate a given dataset, but to devise a model that is able, given a starting and an ending pose, to generate a human-like walking path.

The approach has been investigated with reference to about one thousand walking paths, recorded using a six-camera motion capture system adopted in biomedical posture and motion analysis. A statistical analysis of the errors among the paths generated by the identified optimal control problem and the experimental paths confirmed that the cost functions here proposed, compared to other cost functions presented in the literature, allow to achieve a significant improvement in the reproduction of the human walking paths. In addition, the cost functions here proposed are simpler and allow for a more intuitive and physically-grounded interpretation.

It is worth mentioning that this improvement is not only due to the proposed cost function. Indeed, one of the major contributions of this work is to consider the problem in the space domain. This choice allows for a simplification in the solution of the inverse optimal control problem, and represents a significant difference with respect to previous approaches, e.g. [3, 30, 35].

On the other hand, this work does not aim at proposing a methodology to solve a generic inverse optimal control problem as on this specific topic a huge amount of literature exists (the interest reader can make reference, e.g., to [10, 14, 16, 21, 23, 25, 42]).

The paper is organised as follows. First, a review of the literature is discussed in Section 2. The problem statement is outlined in Section 3. Section 4 describes the experimental setup used to collect human walking paths. In Section 5 the reformulation of the locomotor model in the space domain is introduced, and some cost functions are proposed and discussed. In Section 6 the solution of the inverse optimal control problem is outlined. Section 8 presents a comparison, based on the experimental paths, among the three cost functions described in Section 5 and among the results obtained with the time and space formulations. Some conclusions are given in Section 9.

2 Review of the literature

An optimal control approach has been formerly applied in the field of neuroscience [43] to predict motion of limbs, i.e., by searching a control input according to some performance criterion, such as minimization of jerk [46], torque-change [45], maximization of smoothness [19], [44], and so forth.

Such an approach has been first adopted in [6], just to find the underlying principle explaining the shape of human walking trajectories. First of all, they assumed that goal-directed walking may be planned as a whole at trajectory level, rather than on successive footsteps. This implies that all biomechanical issues related to motion generation can be neglected. As a consequence, they assumed a purely kinematic model of human locomotion in the form of a unicycle model, extended to make the curvature a state variable, in order to prevent curvature discontinuities. Finally, they assumed the minimization of the control energy as the optimality criterion, which comes down to the minimization of the time derivative of the curvature for "reasonably" constant forward velocities (this hypothesis has been confirmed by a statistical analysis). Clothoid arcs were obtained as the geometric shapes of the walking trajectories from the solution of the optimal control problem, i.e., minimum-length continuous curvature paths under a centripetal peak-jerk constraint[1]. The locomotor model has been further extended in [29] with an additional holonomic (orthogonal) acceleration input, to account for sidewards motion. The cost function has been also modified with the inclusion of the total time, and its weights have been selected based on empirical observations and numerical investigations, while anyway penalizing the holonomic motion, except for near targets and similar initial and final orientations.

In [6] and [30] the authors assume that decisions are optimal with respect to a certain (unknown) cost function, and try to minimize the difference between what is observed and what would have been observed given a candidate cost function. The cost function is represented as a linear combination of basis functions weighted by an unknown parameter vec-

---

[1] This conclusion has been however the subject of some criticisms in [11].

tor. Their approach infers the parameter vector, solves the corresponding optimal control problem, predicts what the resulting observations would be, and then applies derivative-free optimization to minimize the difference between predicted and observed trajectories. This approach, however, is computationally expensive as it requires solving an optimal control problem at each iteration of the optimizer.

Other approaches are presented in [17], in which the authors implement several algorithms, based on inverse reinforcement learning, that do not require solving the forward problem, and in [13, 39], where statistical analysis is applied over a set of recorded human trajectories, in order to extract a low dimensional linear model of human walking trajectory planning. In particular, in [13] Principal Component Analysis has been applied, showing that the span of in-training human paths can be reasonably approximated by a linear subspace of five modes only, while in [39] a statistical technique based on multilinear algebra has been performed for studying heterogeneous databases of human motion behaviors.

3 Problem statement

It must be emphasized that, in all reviewed approaches, the focus is on the geometric shape of the human walking trajectories and, in this respect, the role of the forward velocity should be put in question. On the one hand, it has been observed that the forward velocity remains nearly constant along the trajectories [6] (a constant forward velocity has been even explicitly assumed in [9]). On the other hand, recently, Mombaur et al. [30] have noticed that the objective function of human locomotion trajectories does not seem to depend on the forward velocity, and the same observation has been made for the jerk. Accordingly, it appears reasonable to assume that a human being plans the shape of her/his trajectory in the space domain, moving along it at a velocity consistent with her/his particular biomechanical characteristics. Indeed, it has been observed from the experiments that different subjects follow similar paths with fairly different velocities.

This fact has suggested a reformulation of the unicycle model in the space domain, assuming the natural coordinate as the independent variable instead of time.

Apart from removing the dependence from the forward velocity and lowering the number of model inputs to one, the said reformulation has the advantage of avoiding the need of rescaling the trajectories [6, 13, 39] since, of course, even from trial-to-trial, the duration of the motion performed by different subjects can be different, while producing similar paths. Moreover, the only input of the reformulated model is actually the curvature, whose continuity is assured by the solution of the optimal control problem itself, rather than

from an extension of the unicycle model in order to make the curvature a state variable [4, 6, 9].

According to the space domain reformulation of the motion model, in this work walking paths instead of walking trajectories are considered in the search of an optimality criterion, adapting the approach proposed in [26, 35] and already considered in [32]. This new formulation of inverse optimal control assumes that the observations are perfect, while the system is considered to be only approximately optimal. This allows to define residual functions based on the Karush-Kuhn-Tucker (KKT) necessary conditions for optimality [28]. Then, the inverse optimal control problem can be solved by minimizing these residual functions, recovering the parameters that govern the cost function. As a result, the inverse optimal control problem reduces to a simple least-squares minimization, which can be solved very efficiently.

This approach is also similar to the "analytical" one presented in [42], which exploits the Lagrange principle – thus analogous to the necessary conditions of optimality of the KKT – and solves the weights in closed form. This method is proven to converge always to a unique global minimum in the case of linear constraints, reaching very accurate approximations of the true cost function, while being 300 times faster than other classical approaches. Unfortunately, due to the nonlinearity in the dynamics of the walking person, the resulting optimization problem cannot be formulated with linear constraints.

From the discussion above, it should be clear that there are two key aspects that have to be considered in order to address the planning problem.

First, as the problem of selecting a suitable cost function given a set of experimental paths, can be considered as an identification problem, collecting a dataset of human walking paths is a fundamental step. Therefore, the first part of this paper is dedicated to the description of the experimental setup used for the process of human path recording.

Second, as the identified cost function should be somehow general, and not just tailored on the considered set of experimental paths, in the authors' opinion the procedure adopted to select the structure and weights of this cost function should guarantee that the optimality criterion has a straightforward physical interpretation.

4 Collecting human walking paths

As previously mentioned, collecting human walking paths is a preliminary but fundamental aspect of this work. In this section, the experimental setup used to collect the dataset is thus described.

About one thousand paths were recorded using a six-camera motion capture system (SMART system by BTS S.p.A.). Each subject was equipped with 3 light reflective markers,

two located on the hips – anterior superior iliac spine (asis) –, and one located on the sacrum (Figure 1). This is not the optimal placement of markers in order to minimize the oscillations induced by step alternation, in this respect the shoulders' midpoint would be a better choice [3, 30], but the consequences of this choice on the regularity in the reconstruction of motion were anyway negligible.
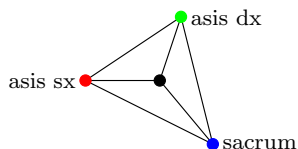

Fig. 1: Marker positions and barycenter.

The experimental protocol was inspired to the one adopted in [6]. More specifically, the study is restricted to the "natural" forward locomotion, excluding goals located behind the starting position and goals requiring side-walk steps.
Goals are defined both in position and orientation, and in order to cover at best the accessibility region, a 4m×6m rectangle corresponding to the calibrated volume, was sampled with 144 points defined by 12 positions on a 2D grid (left side of Figure 2) and 12 orientations each. The final orientation varied from 0 to 2π in intervals of $\pi/6$ at each final position (right side of Figure 2). The starting position and orientation were always the same (they are shown by a small arrow in the 2D grid of Figure 2).
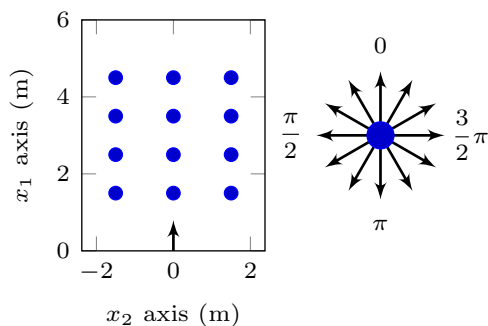

Fig. 2: Final porch positions (left) and orientations (right).

Locomotor trajectories of 7 healthy people (both males and females), who volunteered for participation in the experiments, were recorded. Their ages, heights, and weights ranged from 24 to 50 years, from 1.60 to 1.85m, and from 50 to 90kg, respectively. Each subject performed all the 144 trajectories. Subjects walked from the same initial configuration to a randomly selected final configuration. The target consisted of a porch that could be rotated around a fixed
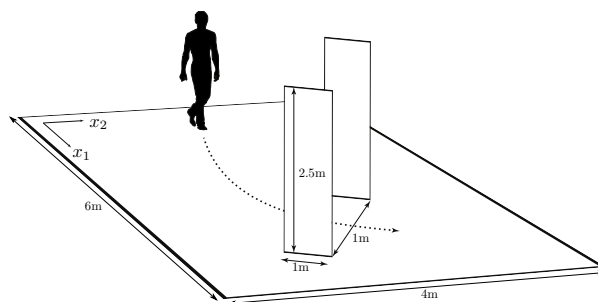

Fig. 3: An example of experiment.

position in order to show the desired final orientation (Figure 3).
The subjects were instructed to freely cross over this porch without any spatial constraint relative to the path they might take. Further, they were allowed to choose their natural walking speed to perform the task. It is worth noticing that the trajectory was recorded starting from the time instant when the subject crossed the $(0,0)$ position in Figure 2. This was done in order to limit as much as possible holonomic behaviors that may arise in the case of the closer targets [30].

A pre-processing phase on the paths collected by the optoelectronic system was required in order to remove outliers, fill in missing data and smooth the curves, interpolating each marker with a smoothing spline. Then, considering the triangle that the three markers form (Figure 1), the path of a unique "virtual" marker representing the human walking path was computed as the barycenter of said triangle.

5 Walking path generation using optimal control

In the framework just introduced, the problem of planning human walking paths can be formulated as an optimal control problem, whose dynamic model and cost function have to be selected in such a way that the planned paths are human-like, i.e., resemble the paths walked by a human. These two fundamental aspects, i.e., the selection of the walking model and of the cost function, are discussed in detail in this section.

5.1 Locomotion model

A walking human can be represented by a rectangular box (Figure 4), that can translate and rotate around an axis parallel to the vertical dimension of the box, and crossing the base in its center.
The pose of the human is thus completely described by the coordinate of the rectangular box base center P, with respect to a reference frame fixed on the ground plane, and by the angle formed by the tangent to the walking path with the
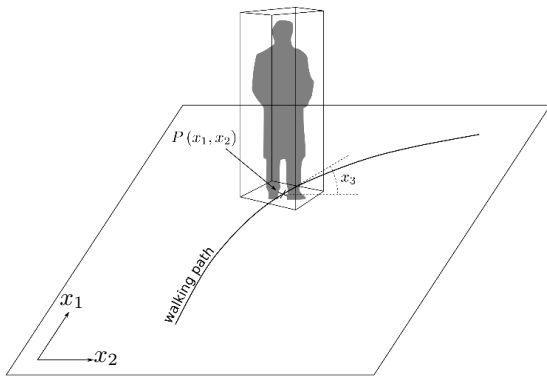
Fig. 4: Formalization of a human walking path.

x_1-axis. Then, a human walking path is defined as the curve followed by the point P through the ground plane.

As far as human path planning is concerned, the complex activities performed during walking by muscles and brain in commanding and coordinating many elementary motor acts can be neglected, and the problem may be considered from a high-level kinematic model perspective. Following this approach, the walking human can be modeled [3, 35] with the unicycle kinematic model

$$\begin{cases} \dot{x}_1 = v\cos(x_3) \\ \dot{x}_2 = v\sin(x_3) \\ \dot{x}_3 = \omega \end{cases} \tag{1}$$

where x_1, x_2 are the Cartesian coordinates of point P, v is the linear (nonholonomic) velocity along the direction of motion, x_3 is the orientation, and ω is the angular velocity.

A solution of the unicycle kinematic model (1) represents a trajectory in the Cartesian space, including thus the geometry of the path and the position of point P over time, as well.

In the authors' opinion, however, the problem of generating human-like walking paths should be addressed focusing only on the geometry of the path, instead of the complete trajectory as a function of time. In fact, the forward velocity v can vary with time along the path and it depends on a large number of factors [27, 31]. As an example, a statistical analysis of the dataset presented in Section 4 shows that the average and median walking velocity are very close, i.e., 1.12m/s and 1.14m/s, respectively, but the walking velocity, even neglecting possible outliers, spans the range $0.61 - 1.69$m/s, exhibiting thus a very high variance.

Furthermore, in the absence of obstacles and environmental stimuli that can trigger unpredictable human reactions, the velocity v can be considered independent from the geometry of the path, as at walking velocity the inertial effects are almost negligible.

For these reasons, the remaining of this work is focused on planning only the geometry of the path, assuming that once a human-like path has been generated, one can superimpose on this path any desired velocity profile, just holding the constraint of "natural walking" introduced in [6]. In addition, leaving out from the estimation the forward velocity, in principle, reduces the dimension of the inverse optimal control problem, thus making its solution easier and more reliable [14, 23].

In order to study the geometry of the path, model (1) can be rewritten with the natural coordinate s as the independent variable, avoiding the explicit dependence of the model from the velocity v, and lowering the number of input variables to one. Thus, if $v > 0$ along the path, i.e., if the assumption of "natural walking" introduced in [6] holds, the relation between the natural coordinate s and time t is given by

$$s(t) = \int_0^t v(\tau)\,\mathrm{d}\tau$$

and can be inverted, defining $t = t(s)$. As a consequence, model (1) can be rewritten as

$$\begin{cases} x_1' = \cos(x_3) \\ x_2' = \sin(x_3) \\ x_3' = \sigma \end{cases} \tag{2}$$

where $\sigma = \omega/v$ is a new input variable, and the notation $'$ represents the derivative with respect to the natural coordinate s: $x' = \mathrm{d}x/\mathrm{d}s$.

Considering now how complex are the activities performed during walking, but how simple are models (1) and (2) herein introduced, a question naturally arises: is the unicycle model well-suited to describe the dynamics of a human that is walking in a free space? Or, alternatively, should it be improved, adding the curvature as a further state variable, as proposed in $[4,6,9]^2$?

In order to reply to this question, it must be first noticed that in [4, 6, 9] the authors extended the unicycle model (1), including the path curvature as a further state variable, in order to enforce its continuity along the path.

Considering the unicycle model in the space domain (2), however, it can be easily verified that the path curvature κ has the following expression

$$\kappa = \left| \frac{x_1' x_2'' - x_2' x_1''}{\left(x_1'^2 + x_2'^2\right)^{\frac{3}{2}}} \right| = \left| \frac{x_3' \cos^2(x_3) + x_3' \sin^2(x_3)}{\left(\sin^2(x_3) + \cos^2(x_3)\right)^{\frac{3}{2}}} \right| = |x_3'|$$

being thus equal to the absolute value of the quantity σ, that in the optimal control problem plays the role of the control variable.

Further, under mild assumptions concerning the continuity and differentiability of the model equations and of the cost

---

[2] Note that, considering the assumption of natural forward locomotion, the unicycle and the extended unicycle are the only models that appeared in the literature on planning human walking paths.

function, it can be proved that the solution of the optimal control problem, i.e., the optimal state and control trajectories, is continuous [20]. The same conclusion can be drawn even when state constrained problems are considered and/or when the optimal control is constrained, assuming that it belongs to a convex set.

As a consequence, if one considers the walking model in the space domain, there is no need to introduce an extended model, as even the simplest one, i.e., model (2), thanks to the properties of the solution of the optimal control problem, ensures the continuity of the path curvature.

On the other hand, in order to experimentally assess the validity of model (2), each experimental path has been compared with the corresponding one obtained integrating the model fed by the velocities computed using the experimental data. This comparison was based on the Fréchet metric [2], that the authors consider the best way to measure the geometrical difference between two curves—a deeper discussion is presented in Section 7.
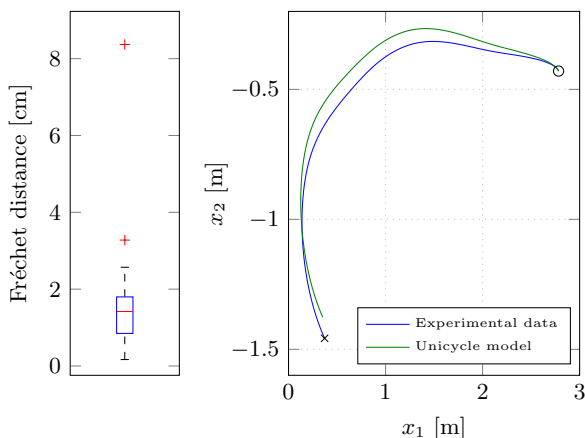

Fig. 5: A comparison between the paths generated using the unicycle model and the experimental paths: on the left side the box-plot of the validation error, on the right side the simulated (green line) and experimental (blue line) paths corresponding to the worst outlier. The 'o' and 'x' indicate the initial and final position, respectively.

Fréchet distance [cm]		
25th Percentile	Median	75th Percentile
0.84785	1.4176	1.7982

Table 1: Statistical validation of the unicycle model.

Figure 5 and Table 1 show the results of a statistical comparison between the unicycle model (2) and the path dataset introduced in Section 4. As it is clearly shown by the values

reported in Table 1, the error is almost negligible, in particular as it is very close to the resolution of the motion capture system. The slight difference between the paths generated by the model and the experimental one is also evident in the left side of Figure 5, where a path, corresponding to the worst outlier pointed out by the statistical analysis, is compared with the corresponding experimental one.

5.2 Choosing the cost function

The multiplicity of different approaches to human planning as an optimal control problem that have been devised in the literature [3, 6, 9, 10, 32, 35] reveal that the choice of the cost function is the most critical issue. In fact, apart from obvious criteria such as minimization of the energy consumption or minimization of the distance and the derivative of the curvature, the way humans plan walking paths depends in general from the situation, from environmental constraints and stimuli, etc.

As already discussed in Section 3, this work is focused on the definition of a cost function that, apart from obviously being experimentally validated, it should be physically grounded and as simple as possible. To this extent, three different cost functions are presented in the following.The results achievable with such cost functions, in generating a human-like walking path, are compared in Section 8.

5.2.1 Energy-based cost function

In [3, 6, 9, 35] an energy-based (EB) cost function was proposed. Considering the unicycle model in the time domain (1), this cost function can be rewritten in continuous time as follows

$$J = \frac{1}{2} \int_0^T \left(\alpha v^2 + \omega^2 \right) dt \qquad (3)$$

where T is the duration of the trajectory, and α is an unknown parameter that has to be estimated through the solution of an inverse optimal control problem. This parameter governs how much we penalize control effort v relative to control effort ω.

As previously mentioned, the cost function introduced in [3, 6, 9, 35] is related to the energy needed to perform the path, and the underlying rationale is that humans wants to minimize it.

5.2.2 Hybrid energy/goal-based cost function

Following the same approach already introduced in [35], in [32] the authors proposed a new cost function, that is based on the space domain unicycle model (2), and accounts either for the energy related to the control effort σ, and for the distance between the current state and the final state.

This cost function, we refer to as the hybrid energy/goal-based (HEGB), can be formulated in continuous time as follows

$$J = \frac{1}{2} \int_0^S \sigma^2 \left(1 + \beta^T \Gamma^2\right) ds \qquad (4)$$

where S is the length of the path, $\beta^T = \begin{bmatrix} \beta_1 & \beta_2 & \beta_3 \end{bmatrix}$ is a set of unknown parameters that need to be estimated through the solution of an inverse optimal control problem, and

$$\left(\Gamma^2\right)^T = \left[\left(x_1 - x_{1_g}\right)^2 \ \left(x_2 - x_{2_g}\right)^2 \ \left(x_3 - x_{3_g}\right)^2 \right]$$

$(x_{1_g}, x_{2_g}, x_{3_g}) =: \mathbf{x}_g$ being the final pose of the human.
The rationale behind this cost function is that the distance of the current state from the goal can be interpreted as a space-varying weight on the control effort σ.

5.2.3 Normalized hybrid energy/goal-based cost function

A new cost function, is here considered, with the aim of simplifying the identification of the β parameters, and of improving the quality of the planned walking paths.
To this extent, two changes are introduced:

1. a reduction of the number of parameters, weighting the Euclidean distance from the actual to the final human position instead of separately weight the x_1- and x_2-distances;
2. a normalisation of the Euclidean and angular distances with respect to their boundary values.

The modified cost function, we refer to as the normalized hybrid energy/goal-based (NHEGB), can be thus formulated as follows

$$J = \frac{1}{2} \int_0^S \sigma^2 \left(1 + \gamma^T \tilde{\Gamma}^2\right) ds \qquad (5)$$

where $\gamma^T = \begin{bmatrix} \gamma_1 & \gamma_2 \end{bmatrix}$ is a set of unknown parameters that need to be estimated through the solution of an inverse optimal control problem, and

$$\left(\tilde{\Gamma}^2\right)^T = \left[\frac{\left(x_1 - x_{1_g}\right)^2 + \left(x_2 - x_{2_g}\right)^2}{\left(x_{1_s} - x_{1_g}\right)^2 + \left(x_{2_s} - x_{2_g}\right)^2} \ \frac{\left(x_3 - x_{3_g}\right)^2}{\left(x_{3_s} - x_{3_g}\right)^2} \right]$$

$(x_{1_s}, x_{2_s}, x_{3_s}) =: \mathbf{x}_s$ and $(x_{1_g}, x_{2_g}, x_{3_g}) =: \mathbf{x}_g$ being the initial and final pose of the human, respectively.

6 Solving the Inverse Optimal Control problem

This section introduces the methodology used to solve the inverse optimal control problem. This methodology extends the work in [35], by suitably adapting and applying the solution of the inverse optimal control problem to the proposed cost functions.

First of all, model (2) can be discretised yielding

$$\begin{cases} x_1(k+1) = x_1(k) + \Delta s(k) \cos\left(x_3(k)\right) \\ x_2(k+1) = x_2(k) + \Delta s(k) \sin\left(x_3(k)\right) \\ x_3(k+1) = x_3(k) + \Delta s(k) \sigma(k) \end{cases} \qquad (6)$$

where $\Delta s(k) = s(k) - s(k-1)$ is a discrete space step, and k is not a time, but a space index.
Considering, for the sake of an example, the cost function (4), the inverse optimal control problem can be formulated as follows

$$\begin{aligned} \min_{\mathbf{x}(k), \sigma(k)} \quad & \frac{1}{2} \sum_{k=0}^{N-1} \sigma(k)^2 \left(1 + \beta^T \Gamma^2\right) \Delta s(k) \\ \text{s.t.} \quad & \mathbf{x}(0) - \mathbf{x}_s = 0 \\ & \mathbf{x}(N-1) - \mathbf{x}_g = 0 \\ & x_1(k+1) - \left[x_1(k) + \Delta s(k) \cos\left(x_3(k)\right)\right] = 0 \\ & x_2(k+1) - \left[x_2(k) + \Delta s(k) \sin\left(x_3(k)\right)\right] = 0 \\ & x_3(k+1) - \left[x_3(k) + \Delta s(k) \sigma(k)\right] = 0 \\ & \forall k = 0, \dots, N-1 \end{aligned} \qquad (7)$$

where $\mathbf{x} = \begin{bmatrix} x_1 & x_2 & x_3 \end{bmatrix}^T$ is the state vector, $\mathbf{x}_s$ and $\mathbf{x}_g$ are the initial and the final states, respectively, and N is the number of samples. The only unknown parameter is vector β, that, together with Γ, acts as a space-varying weight on the control effort σ.

Solving the inverse optimal control problem associated with (7) could be quite complex and computationally inefficient, due to its nonlinearities. For this reason, in [35] a more efficient solution, based on the KKT conditions for optimality, is proposed and here briefly presented.
Let $\chi = \begin{bmatrix} \mathbf{x}^T & \sigma \end{bmatrix}^T$, $f(\chi, \beta) \in \mathbb{R}$ the cost function, and $g(\chi) \in \mathbb{R}^m$ the set of constraints.
For a given β, assuming that $\chi^\star$ is a local minimum of problem (7) and is regular, there exist a unique Lagrange multiplier vector $\lambda^\star \in \mathbb{R}^m$ [28] such that

$$\begin{cases} \nabla_\chi f(\chi^\star, \beta) + \sum_{i=1}^m \lambda_i^{\star T} \nabla_\chi g_i(\chi^\star) = 0 \\ g(\chi^\star) = 0 \end{cases} \qquad (8)$$

provided that $f(\cdot)$ and $g(\cdot)$ are continuously differentiable functions. Equations in (8) are known as the KKT necessary (and sufficient) conditions for equality constraint optimization problems: the first one is the stationarity condition, while the second equation ensures primal feasibility.
The KKT conditions for the Lagrangian of problem (7) can be written as

$$\nabla_{(\chi, \lambda)} \mathscr{L}(\chi, \beta, \lambda) = \nabla_{(\chi, \lambda)} \left(f(\chi, \beta) + \sum_{i=1}^m \lambda_i^T g_i(\chi) \right) = 0$$

Assuming that the system is only "approximately optimal", while observations are perfect, the inverse optimal

control problem can be solved by minimizing the residual function

$$\min_{\beta,\lambda} \quad \frac{1}{2}\|\nabla_{(\chi,\lambda)}\mathscr{L}(\chi,\beta,\lambda)\|^2 = \min_{\beta,\lambda} \quad \frac{1}{2}\|Jz-b\|^2 \qquad (9)$$

where $z = \begin{bmatrix} \beta & \lambda \end{bmatrix}^T$, while J and b depend on the collected data.

The same approach can be followed for each of the cost functions introduced in Section 5.2. The corresponding expressions for J and b are presented in Appendix.

As can be seen, the initial constrained optimization problem (7) has been cast into a convex unconstrained least-squares optimization, which is easier to solve than the initial constrained optimization one, and reads as the classical normal equation, i.e., with the solution $z^\star = J^\dagger b$, where $J^\dagger$ denotes the Moore-Penrose pseudoinverse of J.

One of the main limitations of the approach proposed in [35], is that there is no guarantee that the value of $\beta^\star$ resulting from the normal equation is actually positive. In fact, in many cases, starting from the considered dataset, the solution is a negative value of β, making the optimization problem non-convex.

To overcome this problem, the solution of the normal equation is here taken as the initial guess for the solution of a new optimization problem, i.e., a constrained version of (9), which reads as

$$\min_{\beta,\lambda} \quad \frac{1}{2}\|Jz-b\|^2$$
$$\text{s.t.} \quad \beta \geq 0 \qquad (10)$$

Problem (10) can be easily solved using any optimization software, selecting as initial guess the solution obtained with the normal equation. It is quite intuitive that this modification to the optimization problem (9) is simple yet extremely important.

7 Choosing the performance metric

Another important aspect that must be taken into account is how the performance of different methods are evaluated, i.e., which is the similarity metric that is more suited for the problem.

In the literature, the similarity metric that has been widely adopted is the Euclidean distance [5, 22, 34]. However, with this metric, the comparison of different paths depends on the number of available samples. An extreme case is when two paths generated by two people are compared. Even if the geometry of the path is exactly the same, the computed distance – e.g., the Average Trajectory Errors (ATEs) and Maximal Trajectory Errors (MTEs) [5, 34] – is usually greater than zero, due to the different walking velocities of the two

persons, then due to the different samplings. Even considering a parametrisation of the two trajectories based on the natural coordinate, so as to be invariant with respect to the velocity, is not a viable solution.

Consider, for example, the two curves depicted in Figure 6. They have been compared on the basis of the Root-Mean-Square Error (RMSE), of the ATE and the MTE, using a parametrisation based on the natural coordinate, with or without normalizing the curves with respect to their lengths, and sampling each curve with a resolution of 1 mm, 1 cm, and 1 dm. The resulting distances are reported in Table 2.

Varying the parametrisation the distance changes less than 10%, but comparing the same metric and parametrisation with and without length normalization yields an error greater than 30%. In principle, a good metric should be defined in such a way to be as much invariant as possible with respect to the chosen parametrisation.

For this reason, the Fréchet distance[3], that is by definition independent of the chosen parametrisation, is here adopted to evaluate the similarity between two curves, i.e., to state how good are different models in replicating human walking paths.
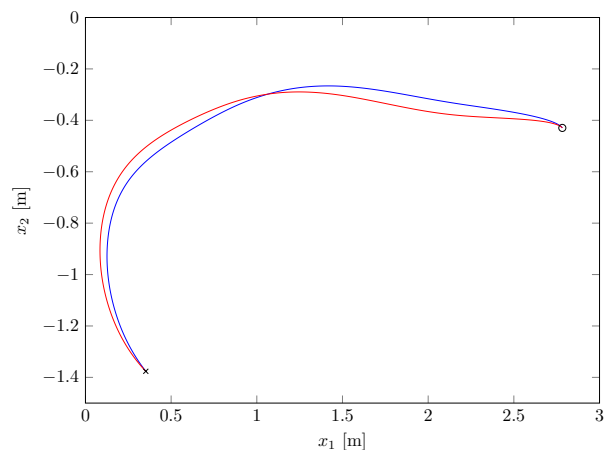

Fig. 6: Two paths used to compare different distance metrics.

Furthermore, the Fréchet distance was indeed adopted to compare parametric curves in different fields, ranging from morphing and handwriting recognition [18], to protein structure alignment [24], but especially in computational geometry [2, 7]. In particular, in [2] it has been proven that the Fréchet distance is a better measure of similarity for curves

---

[3] Given two curves $\phi : [a,b] \to V$ and $\gamma : [a',b'] \to V$, their Fréchet distance is defined as

$$\delta_F(\phi,\gamma) = \inf_{\alpha,\beta} \max_{t \in [0,1]} \quad d(\phi(\alpha(t)),\gamma(\beta(t))) \qquad (11)$$

where α and β are arbitrary continuous non-decreasing function from $[0,1]$ onto $[a,b]$ and $[a',b']$ respectively.

Metric	Distance [mm]
RMSE sampling 1 mm	37.59
RMSE sampling 1 cm	37.56
RMSE sampling 1 dm	37.29
RMSE sampling 1 mm, normalized length	47.13
RMSE sampling 1 cm, normalized length	46.92
RMSE sampling 1 dm, normalized length	44.93
ATE sampling 1 mm	34.27
ATE sampling 1 cm	34.49
ATE sampling 1 dm	36.58
ATE sampling 1 mm, normalized length	44.00
ATE sampling 1 cm, normalized length	43.99
ATE sampling 1 dm, normalized length	43.42
MTE sampling 1 mm	50.00
MTE sampling 1 cm	49.99
MTE sampling 1 dm	49.91
MTE sampling 1 mm, normalized length	69.60
MTE sampling 1 cm, normalized length	69.59
MTE sampling 1 dm, normalized length	69.59
Fréchet	49.99

Table 2: Comparison between different distance metrics.

than other alternatives, such as the Hausdorff distance, for arbitrary point sets.

Though the computation of this distance is not trivial, there are some efficient techniques to determine its discrete counterpart over a polygonal curve, which has been proven to be converging to (11) as the number of points goes to infinity [2].

8 Experimental results

This section presents a comparison, based on the experimental paths introduced in Section 4, among the three cost functions described in Section 5.2.

The geometry of two curves is here compared using the Fréchet metric.

In order to obtain a general cost function that can be used for all the possible couple of initial and final position and orientation different approaches can be adopted. In [42], the authors compute the residual for each experiment, and they compute the weights through the solution of least squares optimization for all of the residuals jointly. However, adopting this approach would mean losing the advantage of solving the inverse optimal control problem as the solution of a system of linear equations. In [30], the general cost function is obtained on the basis of 5 "scenarios", i.e., 5 prescribed initial and goal conditions, and of 5 subjects, for a total of 25 trajectories out of the 2040 trajectories available in their dataset. Still in [30], the authors performed also experiments with only a single scenario for 5 subjects (out of the 10 considered in their study) and they obtained that the "resulting parameters in all cases were very similar".
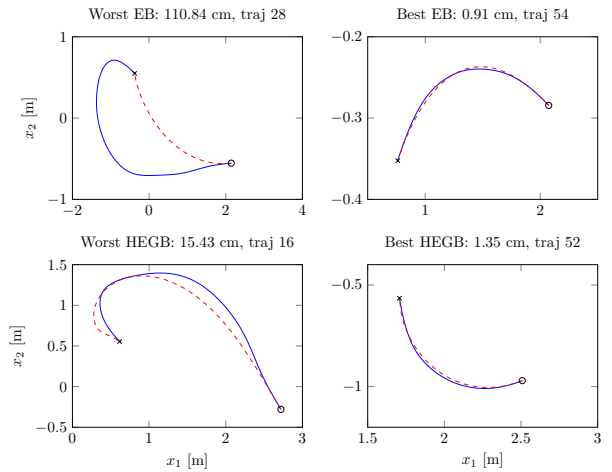

Fig. 7: The best and the worst path generated with the EB and with the HEGB approaches. The solid lines represent the experimental paths, the dashed lines are the optimal EB and HEGB solutions, and the 'o' and 'x' indicate the initial and final position, respectively.
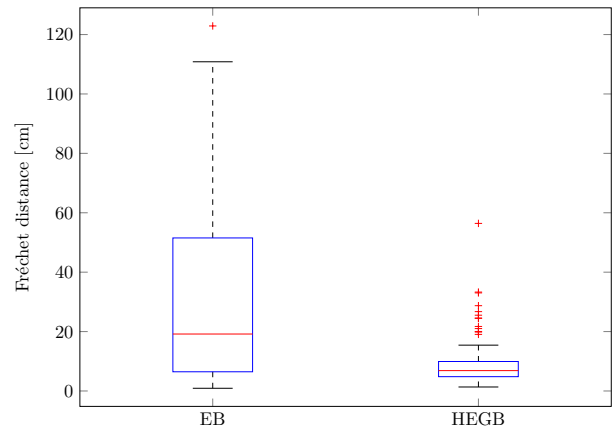

Fig. 8: Statistical analysis (box-plot) of the distance between each generated path and the corresponding experimental one.

In this work, we choose to obtain the general cost function as follows. For each trajectory in the dataset, the optimal value of the parameters is estimated by solving the inverse optimal control problem, considering all the subjects in the study. Then, the average of the weights is computed, see Table 3. Then, the solution of the (direct) nonlinear optimization problem (10) is performed using an interior point algorithm [28], and the the cost function with the computed average of the weights. Other studies in the literature have used a similar approach, e.g., [4, 6, 35].

It is worth noticing that the average of the weights is not the solution to *any* of the solved inverse optimal control problems, but is a generalization of the obtained weights. The results presented in this section are thus in validation,

	Cost function parameters					
	α	β_1	β_2	β_3	γ_1	γ_2
Energy-based	0.06	-	-	-	-	-
Hybrid energy/goal-based	-	125	42.47	190	-	-
Normalized hybrid energy/goal-based	-	-	-	-	7.55	0.27

Table 3: Parameters of the cost functions introduced in Section 5.2 estimated from the experimental dataset.
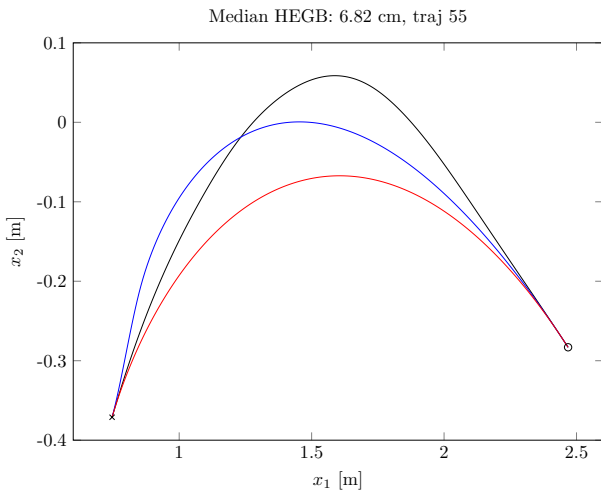

Fig. 9: A comparison among the paths, corresponding to the median distance error, generated with the EB (red line) and the HEGB (black line) approach and the corresponding experimental path (blue line). The 'o' and 'x' indicate the initial and final position, respectively.

proving that the robustness of the proposed methodology is quite high with respect to the chosen weights, that the sensitivity of the weights is fairly low, and also that there is no overfitting.

First, we consider and compare the paths generated with the EB and HEGB methods. From Figure 7 it is apparent that the EB solution is not able to reliably reproduce the collected data. Indeed, though Figure 7 shows only the paths which are characterized by the minimum and the maximum error with respect to the experimental ones, this kind of behaviour is also present in many other optimized trajectories, omitted here for space limitations. A concise representation of the performance of the method presented in [35], in reproducing the dataset considered herein, is given by the statistical analysis of the distance between each generated path and the corresponding experimental one (Figure 8) and by the comparison of the paths that give rise to the median distance (Figure 9).

It is opinion of the authors that this kind of error in reproducing the experimental paths is not only due to the fact that the chosen value of the cost function parameter α is not the optimal one, but also to the selected cost function (3) which is inherently not able to replicate the human way of
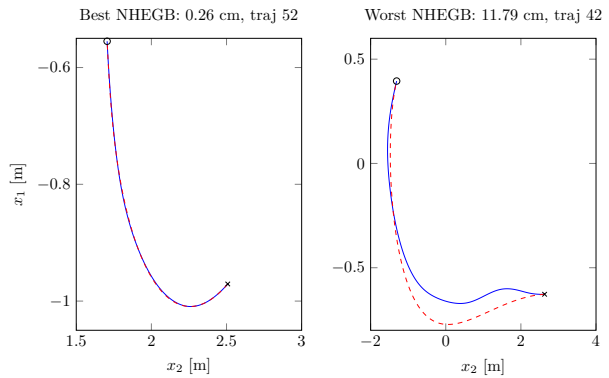

Fig. 10: The best and the worst path generated with cost function (5). The blue lines represent the experimental paths, the 'o' and 'x' indicate the initial and final position, respectively.
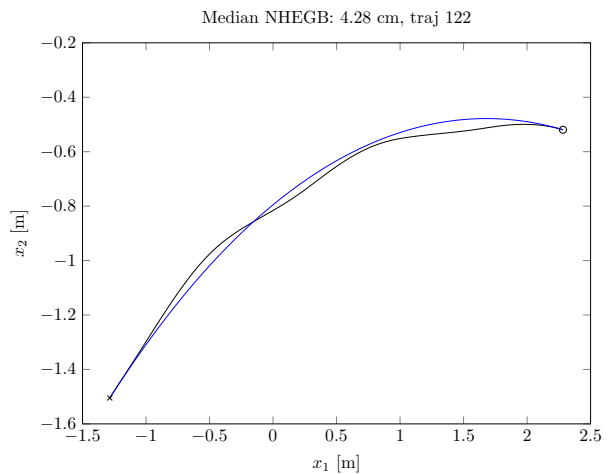

Fig. 11: A comparison between the path, corresponding to the median distance error, generated with cost function (5) (black line) and the corresponding experimental path (blue line). The 'o' and 'x' indicate the initial and final position, respectively.

planning paths.

In some cases both the EB and the HEGB methods manage to reproduce the human path, but also in those cases the HEGB method seems to be closer. There are also several other cases, however, in which the EB method fails. The performance improvement achieved by the cost function (4) is apparent, either from a qualitative comparison
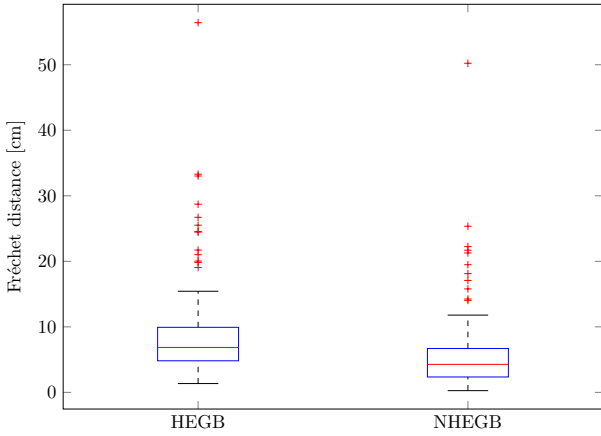
Fig. 12: Statistical analysis (box-plot) of the distance between each path, generated with the *space* method and with cost function (5), and the corresponding experimental one.

Fig. 13: Close targets

Fig. 14: Porch at π orientation.

among the paths generated by the two approaches and the corresponding experimental ones (Figure 7), and from the statistical analysis of the error distances (Figure 8). Further, the Fréchet distance between the generated path and the experimental one (Figure 7) shows that the HEGB method outperforms the EB approach in the worst case and in the best case as well.

The results achieved with the HEGB approach, can be further improved by the cost function (5) herein proposed. The reduction of the distance error is apparent from the qualitative analysis of the best and the worst path (Figure 10), and of the path corresponding to the median distance error (Figure 11).
Further, the quantitative analysis shows that the Fréchet distance between the generated path and the experimental one has been reduced, with respect to the HEGB method, of 20% in the case of the worst path and 80% for the best path (Figures 7 and 10).
Finally, the statistical analysis (Figure 12) confirms that the previous conclusions hold for the whole dataset. As it is clearly shown by the comparison between the box-plots obtained with the HEGB and with the NHEGB approaches, whatever distance measure is considered, the last one yields a significant improvement in the reproduction of the human walking paths.

In order to make the comparison between the three cost functions herein analysed more clear, the results of the statistical analysis of the distances between each generated path and the corresponding experimental one are summarized in Table 4.
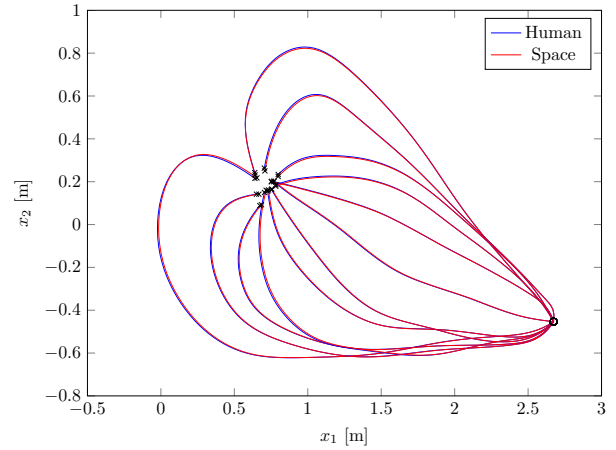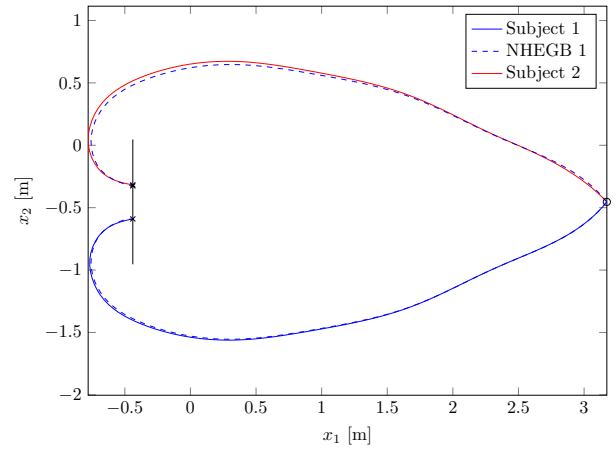
8.1 Discussion

In addition to the presented results, there are some other important aspects that are worth discussing. The first problem is how the model behaves in the case of "close targets". In fact, in [30] it was proven that in the case of targets really closed to the initial position, the nonholonomic assumption may not hold. In this respect, it must be recalled from Section 4, that the subjects started walking before entering in the calibrated volume, thus the initial velocity was greater than zero. As a consequence, the holonomic assumption holds from the beginning of the motion.
Figure 13 shows the trajectories for a single target, a single subject, with all the orientations. Apparently, the proposed method is able to reproduce accurately all the trajectories.

Another interesting issue is represented in Figure 14. In principle, when the porch is to be crossed with a final orientation of $x_{3_g} = \pi$ (see Figure 2), there are two different solutions that are equivalent both from the cost function and from the kinematic model viewpoint. In the figure, solid

	Fréchet distance [cm]		
	25th Percentile	Median	75th Percentile
Energy-based	6.4652	19.177	51.526
Hybrid energy/goal-based	4.8189	6.8581	9.9262
Normalized hybrid energy/goal-based	2.3489	4.2763	6.6964

Table 4: A comparison between the cost functions introduced in Section 5.2.

lines represent two different paths chosen by the subjects, while dashed lines are the solution of the NHEGB. Apparently the problem itself, for its inherent symmetry, does not have a unique solution, independently of the formulation. In the presented solution, the initial guess is always the human trajectory, therefore the solution to the optimization problem is converging to the same side as the human path. On the other hand, from a practical viewpoint, in these special cases one can just consider the solution that can be obtained on one side, and (easily) compute the symmetric case. For example, if the goal is to avoid the robot to collide with the walking person, the robot can just compute the solution to the optimization problem, and if it is in this situation, just consider also the symmetric case for the planning. Figure 14 shows also the result of this procedure. The NHEGB model has been used for generating the prediction of the trajectory on the bottom and its symmetric has been computed. Apparently, the obtained performance are still really good when compared to the human trajectory.

As a last remark, it is important to remember that main focus of the manuscript is to accurately describe, and thus predict, the human trajectory. The obtained model can be used in different ways. On one hand, one may use such a model to predict the human trajectory in such way to enforce a safer human-robot interaction. However, defining suitable safety regions requires to measure or estimate the velocity of the person and of the robot, and this is a problem that can be solved on top of the trajectory obtained with the presented approach. On the other hand, the model can also be used for the robot motion planning, producing human-like trajectories. The motion planner can generate the shape of the trajectory by solving the optimal control problem, and then decide a suitable velocity for reaching the final goal. Human-like trajectory generation becomes critical for improving the acceptance of robots in working environments, as well as for a safer human-robot interaction [47].

9 Conclusion

An inverse optimal control technique has been applied to investigate the way humans plan their walking paths in a goal-directed motion. While this approach is widely considered in the robotics literature, some novelties are proposed in this work. First of all, the kinematic model has been reformu-

lated in the space domain, assuming the natural coordinate as the independent variable, thus avoiding the dependence from the forward velocity and the need of rescaling the trajectories performed by different subjects. The only input of the reformulated model is just the curvature, which enters directly in the cost function. Then, a recently proposed approach to the solution of the inverse optimal control problem has been adopted, based on simple least-squares minimization. A novel cost function has been also proposed and compared with other cost functions proposed in the literature, adopting the discrete discrete Fréchet distance as a tool to assess the similarity of a set of paths, a metric that was never used for the performance measurement in the context of generation of human walking paths to date. The approach has been investigated with reference to about one thousand walking paths, recorded using a six-camera motion capture system adopted in biomedical posture and motion analysis. A statistical analysis of the errors among the paths generated by the identified optimal control problem and the experimental paths confirmed a significant improvement in the reproduction of the human walking paths.

A Appendix

This appendix reports the calculation of the matrices required to setup the least-squares optimization problem (10), for each of the cost functions introduced in Section 5.2.

A.1 Energy-based cost function

First of all, the unicycle time model in (1) can be discretized yielding

$$\begin{cases} x_1(k+1) = x_1(k) + \Delta t(k)v(k)\cos(x_3(k)) \\ x_2(k+1) = x_2(k) + \Delta t(k)v(k)\sin(x_3(k)) \\ x_3(k+1) = x_3(k) + \Delta t(k)\omega(k) \end{cases} \quad (12)$$

where Δt is the discrete time step, and x_1, x_2, x_3 are the Cartesian coordinates of point P and the orientation, respectively.
Then, considering a discretised version of the cost function (3) and the model in (12), the inverse optimal control problem can be formulated

as follows

$$\min_{\mathbf{x}(k),v(k),\omega(k)} \quad \frac{1}{2}\sum_{k=0}^{N-1}\left(\alpha v(k)^2 + \omega(k)^2\right)\Delta t(k)$$

$$\text{s.t.} \quad \mathbf{x}(0) - \mathbf{x}_s = 0$$
$$\mathbf{x}(N-1) - \mathbf{x}_g = 0$$
$$x_1(k+1) - [x_1(k) + \Delta t(k)v(k)\cos(x_3(k))] = 0 \tag{13}$$
$$x_2(k+1) - [x_2(k) + \Delta t(k)v(k)\sin(x_3(k))] = 0$$
$$x_3(k+1) - [x_3(k) + \Delta t(k)\omega(k)] = 0$$
$$\forall k = 0,\dots,N-1$$

where $\mathbf{x} = \begin{bmatrix} x_1 & x_2 & x_3 \end{bmatrix}^T$ is the state vector, $\mathbf{x}_s$ and $\mathbf{x}_g$ are the initial and the final states, respectively, and N is the number of samples.
Writing, now, the Lagrangian associated with (13), as described in Section 6, the residual functions matrices in (10) become where

$$z = \begin{bmatrix} \alpha & \lambda_1^0 & \lambda_2^0 & \lambda_3^0 & \cdots & \lambda_1^{N-1} & \lambda_2^{N-1} & \lambda_3^{N-1} \end{bmatrix}^T \qquad b = \begin{bmatrix} \zeta(0) \\ \zeta(1) \\ \vdots \\ \zeta(N-1) \end{bmatrix}$$

and

$$J = \begin{bmatrix} \psi(0) & I_{5\times3} & M(0) & \mathbf{0}_{5\times3} & \mathbf{0}_{5\times3} & \cdots & \mathbf{0}_{5\times3} \\ \psi(1) & \mathbf{0}_{5\times3} & -I_{5\times3} & M(1) & \mathbf{0}_{5\times3} & \cdots & \mathbf{0}_{5\times3} \\ \psi(2) & \mathbf{0}_{5\times3} & \mathbf{0}_{5\times3} & -I_{5\times3} & M(2) & \cdots & \mathbf{0}_{5\times3} \\ \vdots & \vdots & \vdots & \vdots & \vdots & \ddots & \vdots \\ \psi(N-1) & \mathbf{0}_{5\times3} & \mathbf{0}_{5\times3} & \mathbf{0}_{5\times3} & \mathbf{0}_{5\times3} & \cdots & -I_{5\times3} \end{bmatrix}$$

with

$$\zeta(k) = \begin{bmatrix} 0 \\ 0 \\ 0 \\ 0 \\ \Delta t(k)\omega(k) \end{bmatrix}, \quad I_{5\times3} = \begin{bmatrix} I_{3\times3} \\ \mathbf{0}_{2\times3} \end{bmatrix}, \quad \psi(k) = \begin{bmatrix} 0 \\ 0 \\ 0 \\ \Delta t(k)v(k) \\ 0 \end{bmatrix},$$

$$M(k) = \begin{bmatrix} 1 & 0 & 0 \\ 0 & 1 & 0 \\ -\Delta t(k)v(k)\sin(x_3(k)) & \Delta t(k)v(k)\cos(x_3(k)) & 1 \\ \Delta t(k)\cos(x_3(k)) & \Delta t(k)\cos(x_3(k)) & 0 \\ 0 & 0 & \Delta t(k) \end{bmatrix}.$$

A.2 Hybrid energy/goal-based cost function

Considering a discretised version of the cost function (4) and the discretized unicycle space model in (6), the inverse optimal control problem can be formulated as follows

$$\min_{\mathbf{x}(k),\sigma(k)} \quad \frac{1}{2}\sum_{k=0}^{N-1}\sigma(k)^2\left(1+\beta^T\Gamma^2\right)\Delta s(k)$$

$$\text{s.t.} \quad \mathbf{x}(0) - \mathbf{x}_s = 0$$
$$\mathbf{x}(N-1) - \mathbf{x}_g = 0$$
$$x_1(k+1) - [x_1(k) + \Delta s(k)\cos(x_3(k))] = 0 \tag{14}$$
$$x_2(k+1) - [x_2(k) + \Delta s(k)\sin(x_3(k))] = 0$$
$$x_3(k+1) - [x_3(k) + \Delta s(k)\sigma(k)] = 0$$
$$\forall k = 0,\dots,N-1$$

where $\mathbf{x} = \begin{bmatrix} x_1 & x_2 & x_3 \end{bmatrix}^T$ is the state vector, $\mathbf{x}_s$ and $\mathbf{x}_g$ are the initial and the final states, respectively, and N is the number of samples.

Writing, now, the Lagrangian associated with (14), as described in Section 6, the residual functions matrices in (10) become

$$z = \begin{bmatrix} \beta^T & \lambda_1^0 & \lambda_2^0 & \lambda_3^0 & \cdots & \lambda_1^{N-1} & \lambda_2^{N-1} & \lambda_3^{N-1} \end{bmatrix}^T$$
$$b = \begin{bmatrix} \zeta(0)^T & \zeta(1)^T & \cdots & \zeta(N-1)^T \end{bmatrix}^T$$

and

$$J = \begin{bmatrix} \psi(0) & I_{4\times3} & M(0) & \mathbf{0}_{4\times3} & \cdots & \mathbf{0}_{4\times3} \\ \psi(1) & \mathbf{0}_{4\times3} & -I_{4\times3} & M(1) & \cdots & \mathbf{0}_{4\times3} \\ \psi(2) & \mathbf{0}_{4\times3} & \mathbf{0}_{4\times3} & -I_{4\times3} & \cdots & \mathbf{0}_{4\times3} \\ \vdots & \vdots & \vdots & \vdots & \ddots & \vdots \\ \psi(N-1) & \mathbf{0}_{4\times3} & \mathbf{0}_{4\times3} & \mathbf{0}_{4\times3} & \cdots & -I_{4\times3} \end{bmatrix}$$

with

$$\zeta(k) = \begin{bmatrix} 0 \\ 0 \\ 0 \\ \Delta s(k)\sigma(k) \end{bmatrix}, \qquad I_{4\times3} = \begin{bmatrix} I_{3\times3} \\ \mathbf{0}_{1\times3} \end{bmatrix}$$

$$\psi(k) = \Delta s(k)\sigma(k)\cdot$$
$$\begin{bmatrix} \sigma(k)\left(x_1(k) - x_{1_g}\right) & 0 & 0 \\ 0 & \sigma(k)\left(x_2(k) - x_{2_g}\right) & 0 \\ 0 & 0 & \sigma(k)\left(x_3(k) - x_{3_g}\right) \\ \left(x_1(k) - x_{1_g}\right)^2 & \left(x_2(k) - x_{2_g}\right)^2 & \left(x_3(k) - x_{3_g}\right)^2 \end{bmatrix}$$

$$M(k) = \begin{bmatrix} 1 & 0 & 0 \\ 0 & 1 & 0 \\ -\Delta s(k)\sin(x_3(k)) & \Delta s(k)\cos(x_3(k)) & 1 \\ 0 & 0 & \Delta s(k) \end{bmatrix}$$

A.3 Normalized hybrid energy/goal-based cost function

Considering a discretised version of the cost function (5) and the discretized unicycle space model in (6), the inverse optimal control problem can be formulated as follows

$$\min_{\mathbf{x}(k),\sigma(k)} \quad \frac{1}{2}\sum_{k=0}^{N-1}\sigma(k)^2\left(1+\gamma^T\tilde{\Gamma}^2\right)\Delta s(k)$$

$$\text{s.t.} \quad \mathbf{x}(0) - \mathbf{x}_s = 0$$
$$\mathbf{x}(N-1) - \mathbf{x}_g = 0$$
$$x_1(k+1) - [x_1(k) + \Delta s(k)\cos(x_3(k))] = 0 \tag{15}$$
$$x_2(k+1) - [x_2(k) + \Delta s(k)\sin(x_3(k))] = 0$$
$$x_3(k+1) - [x_3(k) + \Delta s(k)\sigma(k)] = 0$$
$$\forall k = 0,\dots,N-1$$

where $\mathbf{x} = \begin{bmatrix} x_1 & x_2 & x_3 \end{bmatrix}^T$ is the state vector, $\mathbf{x}_s$ and $\mathbf{x}_g$ are the initial and the final states, respectively, and N is the number of samples.
Writing, now, the Lagrangian associated with (15), as described in Section 6, the residual functions matrices in (10) become

$$z = \begin{bmatrix} \gamma^T & \lambda_1^0 & \lambda_2^0 & \lambda_3^0 & \cdots & \lambda_1^{N-1} & \lambda_2^{N-1} & \lambda_3^{N-1} \end{bmatrix}^T$$
$$b = \begin{bmatrix} \zeta(0)^T & \zeta(1)^T & \cdots & \zeta(N-1)^T \end{bmatrix}^T$$

and

$$J = \begin{bmatrix} \psi(0) & I_{4\times3} & M(0) & \cdots & \mathbf{0}_{4\times3} \\ \psi(1) & \mathbf{0}_{4\times3} & -I_{4\times3} & M(1) & \cdots & \mathbf{0}_{4\times3} \\ \psi(2) & \mathbf{0}_{4\times3} & \mathbf{0}_{4\times3} & -I_{4\times3} & \cdots & \mathbf{0}_{4\times3} \\ \vdots & \vdots & \vdots & \vdots & \ddots & \vdots \\ \psi(N-1) & \mathbf{0}_{4\times3} & \mathbf{0}_{4\times3} & \mathbf{0}_{4\times3} & \cdots & -I_{4\times3} \end{bmatrix}$$

with

$$\zeta(k) = \begin{bmatrix} 0 \\ 0 \\ 0 \\ \Delta s(k)\sigma(k) \end{bmatrix}, \qquad I_{4\times3} = \begin{bmatrix} I_{3\times3} \\ \mathbf{0}_{1\times3} \end{bmatrix},$$

and, letting $\delta_{sg,i} = x_{i_s} - x_{i_g}$, $i \in \{1,2,3\}$ to lighten the notation, the remaining matrices become

$$\psi(k) = \Delta s(k)\sigma(k) \begin{bmatrix} \sigma(k)\dfrac{x_1(k)-x_{1_g}}{\delta_{sg,1}^2+\delta_{sg,2}^2} & 0 \\[2mm] \sigma(k)\dfrac{x_2(k)-x_{2_g}}{\delta_{sg,1}^2+\delta_{sg,2}^2} & 0 \\[2mm] 0 & \sigma(k)\dfrac{x_3(k)-x_{3_g}}{\delta_{sg,3}^2} \\[2mm] \dfrac{\left(x_1(k)-x_{1_g}\right)^2+\left(x_2(k)-x_{2_g}\right)^2}{\delta_{sg,1}^2+\delta_{sg,2}^2} & \dfrac{\left(x_3(k)-x_{3_g}\right)^2}{\delta_{sg,3}^2} \end{bmatrix}$$

$$M(k) = \begin{bmatrix} 1 & 0 & 0 \\ 0 & 1 & 0 \\ -\sigma(k)\sin(x_3(k)) & \sigma(k)\cos(x_3(k)) & 1 \\ 0 & 0 & \sigma(k) \end{bmatrix}$$

References

1. Alami, R., Albu-Schaeffer, A., Bicchi, A., Bischoff, R., Chatila, R., De Luca, A., De Santis, A., Giralt, G., Guiochet, J., Hirzinger, G., et al.: Safe and dependable physical human-robot interaction in anthropic domains: State of the art and challenges. In: Proc. IROS'06 Workshop Physical HumanRobot Interaction(pHRI) in Anthropic Domains, vol. 6. IEEE Press (2006)
2. Alt, H., Godau, M.: Computing the Fréchet distance between two polygonal curves. International Journal of Computational Geometry & Applications **5**(1 and 2), 75–91 (1995). DOI 10.1142/S0218195995000064
3. Arechavaleta, G., Laumond, J.P., Hicheur, H., Berthoz, A.: The nonholonomic nature of human locomotion: a modeling study. In: Biomedical Robotics and Biomechatronics, 2006. BioRob 2006. The First IEEE/RAS-EMBS International Conference on, pp. 158–163 (2006). DOI 10.1109/BIOROB.2006.1639077
4. Arechavaleta, G., Laumond, J.P., Hicheur, H., Berthoz, A.: Optimizing principles underlying the shape of trajectories in goal oriented locomotion for humans. In: IEEE/RAS International Conference on Humanoid Robots, pp. 131–136 (2006). DOI 10.1109/ICHR.2006.321374
5. Arechavaleta, G., Laumond, J.P., Hicheur, H., Berthoz, A.: On the nonholonomic nature of human locomotion. Autonomous Robots **25**(1-2), 25–35 (2008). DOI 10.1007/s10514-007-9075-2
6. Arechavaleta, G., Laumond, J.P., Hicheur, H., Berthoz, A.: An optimality principle governing human walking. IEEE Transactions on Robotics **24**(1), 5–14 (2008). DOI 10.1109/TRO.2008.915449
7. Bai, Y.B., Yong, J.H., Liu, C.Y., Liu, X.M., Meng, Y.: Polyline approach for approximating hausdorff distance between planar free-form curves. Comput. Aided Des. **43**(6), 687–698 (2011). DOI 10.1016/j.cad.2011.02.008
8. Bascetta, L., Ferretti, G., Rocco, P., Ardo, H., Bruyninckx, H., Demeester, E., Di Lello, E.: Towards safe human-robot interaction in robotic cells: an approach based on visual tracking and intention estimation. In: 2011 IEEE/RSJ International Conference on Intelligent Robots and Systems (IROS), pp. 2971–2978 (2011). DOI 10.1109/IROS.2011.6094642
9. Bayen, T., Chitour, Y., Jean, F., Mason, P.: Asymptotic analysis of an optimal control problem connected to the human locomotion. In: Decision and Control, 2009 held jointly with the 2009 28th Chinese Control Conference. CDC/CCC 2009. Proceedings of the 48th IEEE Conference on, pp. 2248–2253 (2009). DOI 10.1109/CDC.2009.5400873
10. Berret, B., Chiovetto, E., Nori, F., Pozzo, T.: Evidence for composite cost functions in arm movement planning: An inverse optimal control approach. PLoS Comput Biol **7**(10), 1–19 (2011). DOI 10.1371/journal.pcbi.1002183
11. Bretl, T., Arechavaleta, G., Akce, A., Laumond, J.P.: Comments on "An optimality principle governing human walking". IEEE Transactions on Robotics **26**(6), 1105–1106 (2010). DOI 10.1109/TRO.2010.2082110
12. Broekens, J., Heerink, M., Rosendal, H.: Assistive social robots in elderly care: a review. Gerontechnology **8**(2), 94–103 (2009). DOI 10.4017/gt.2009.08.02.002.00
13. Castelán, M., Arechavaleta, G.: Approximating the reachable space of human walking paths: a low dimensional linear approach. In: Humanoid Robots, 2009. Humanoids 2009. 9th IEEE-RAS International Conference on, pp. 81–86 (2009). DOI 10.1109/ICHR.2009.5379595
14. Casti, J.: On the general inverse problem of optimal control theory. Journal of Optimization Theory and Applications **32**, 491–497 (1980). DOI 10.1007/BF00934036
15. Ceriani, N., Zanchettin, A., Rocco, P., Stolt, A., Robertsson, A.: A constraint-based strategy for task-consistent safe human-robot interaction. In: Intelligent Robots and Systems (IROS), 2013 IEEE/RSJ International Conference on, pp. 4630–4635 (2013). DOI 10.1109/IROS.2013.6697022
16. Chittaro, F., Jean, F., Mason, P.: On inverse optimal control problems of human locomotion: Stability and robustness of the minimizers. Journal of Mathematical Sciences **195**(3), 269–287 (2013). DOI 10.1007/s10958-013-1579-z
17. Dvijotham, K., Todorov, E.: Inverse optimal control with linearly-solvable MDPs. In: Proceedings of the 27th International Conference on Machine Learning (ICML-10), pp. 335–342. Omnipress (2010). URL http://www.icml2010.org/papers/571.pdf
18. Efrat, Guibas, Har-Peled, S., Mitchell, Murali: New similarity measures between polylines with applications to morphing and polygon sweeping. Discrete & Computational Geometry **28**(4), 535–569 (2002). DOI 10.1007/s00454-002-2886-1
19. Flash, T., Hogan, N.: The coordination of arm movements: an experimentally confirmed mathematical model. The Journal of Neuroscience **5**(7), 1688–1703 (1985). URL http://hdl.handle.net/1721.1/6409
20. Galbraith, G., Vinter, R.: Lipschitz continuity of optimal controls for state constrained problems. SIAM Journal on Control and Optimization **42**(5), 1727–1744 (2003). DOI 10.1137/S0363012902404711
21. Hempel, A., Goulart, P., Lygeros, J.: Inverse parametric optimization with an application to hybrid system control. Automatic Control, IEEE Transactions on **60**(1) (2015). DOI 10.1109/TAC.2014.2336992
22. Hicheur, H., Pham, Q.C., Arechavaleta, G., Laumond, J.P., Berthoz, A.: The formation of trajectories during goal-oriented locomotion in humans. i. a stereotyped behaviour. European Journal of Neuroscience **26**(8), 2376–2390 (2007). DOI 10.1111/j.1460-9568.2007.05836.x
23. Jameson, A., Kreindler, E.: Inverse problem of linear optimal control. SIAM Journal on Control **11**(1), 1–19 (1973). DOI 10.1137/0311001

24. Jiang, M., Xu, Y., Zhu, B.: Protein structure–structure alignment with discrete Fréchet distance. Journal of Bioinformatics and Computational Biology **06**(01), 51–64 (2008). DOI 10.1142/S0219720008003278

25. Kalman, R.E.: When is a linear control system optimal? Journal of Basic Engineering **86**(1), 51–60 (1964). DOI 10.1115/1.3653115

26. Keshavarz, A., Wang, Y., Boyd, S.: Imputing a convex objective function. In: Intelligent Control (ISIC), 2011 IEEE International Symposium on, pp. 613–619 (2011). DOI 10.1109/ISIC.2011. 6045410

27. Knoblauch, R., Pietrucha, M., Nitzburg, M.: Field studies of pedestrian walking speed and start-up time. Transportation Research Record: Journal of the Transportation Research Board **1538**, 27–38 (1996). DOI 10.3141/1538-04

28. Luenberger, D., Ye, Y.: Linear and nonlinear programming, vol. 116. Springer (2008). DOI 10.1007/978-0-387-74503-9

29. Mombaur, K., Laumond, J.P., Yoshida, E.: An optimal control model unifying holonomic and nonholonomic walking. In: Humanoid Robots, 2008. Humanoids 2008. 8th IEEE-RAS International Conference on, pp. 646–653 (2008) DOI 10.1109/ICHR. 2008.4756020

30. Mombaur, K., Truong, A., Laumond, J.P.: From human to humanoid locomotion–an inverse optimal control approach. Autonomous Robots **28**, 369–383 (2010). DOI 10.1007/ s10514-009-9170-7

31. Öberg, T., Karsznia, A., Öberg, K.: Joint angle parameters in gait: reference data for normal subjects, 10–79 years of age. Journal of Rehabilitation Research and Development **31**(3), 199–213 (1994). URL http://www.ncbi.nlm.nih.gov/pubmed/7965878

32. Papadopoulos, A., Bascetta, L., Ferretti, G.: Generation of human walking paths. In: Intelligent Robots and Systems (IROS), 2013 IEEE/RSJ International Conference on, pp. 1676–1681 (2013). DOI 10.1109/IROS.2013.6696574

33. Papadopoulos, A.V., Bascetta, L., Ferretti, G.: A comparative evaluation of human motion planning policies. In: Proceedings of the 19th IFAC World Congress, vol. 19, pp. 12,299–12,304 (2014). DOI 10.3182/20140824-6-ZA-1003.01898

34. Pham, Q.C., Hicheur, H., Arechavaleta, G., Laumond, J.P., Berthoz, A.: The formation of trajectories during goal-oriented locomotion in humans. ii. a maximum smoothness model. European Journal of Neuroscience **26**(8), 2391–2403 (2007). DOI 10.1111/j.1460-9568.2007.05835.x

35. Puydupin-Jamin, A.S., Johnson, M., Bretl, T.: A convex approach to inverse optimal control and its application to modeling human locomotion. In: Robotics and Automation (ICRA), 2012 IEEE International Conference on, pp. 531–536 (2012). DOI 10.1109/ ICRA.2012.6225317

36. Ragaglia, M., Bascetta, L., Rocco, P.: Multiple camera human detection and tracking inside a robotic cell an approach based on image warping, computer vision, k-d trees and particle filtering. In: 11th International Conference On Informatics in Control, Automation and Robotics ICINCO 2014, pp. 374–381 (2014)

37. Ragaglia, M., Bascetta, L., Rocco, P.: Detecting, tracking and predicting human motion inside an industrial robotic cell using a map-based particle filtering strategy. In: International Conference on Advanced Robotics ICAR 2015 (2015)

38. Ragaglia, M., Bascetta, L., Rocco, P., Zanchettin, A.: Integration of perception, control and injury knowledge for safe human-robot interaction. In: IEEE International Conference on Robotics and Automation ICRA 2014, pp. 1196–1202 (2014)

39. Ramirez, C.A., Castelán, M., Arechavaleta, G.: Multilinear decomposition of human walking paths. In: IEEE-RAS International Conference on Humanoid Robots, pp. 492–497 (2010). DOI 10.1109/ICHR.2010.5686313

40. Schiavi, R., Bicchi, A., Flacco, F.: Integration of active and passive compliance control for safe human-robot coexistence. In: Robotics and Automation, 2009. ICRA '09. IEEE International Conference on, pp. 259–264 (2009). DOI 10.1109/ROBOT.2009. 5152571

41. Sisbot, E., Marin-Urias, L., Alami, R., Simeon, T.: A human aware mobile robot motion planner. Robotics, IEEE Transactions on **23**(5), 874–883 (2007). DOI 10.1109/TRO.2007.904911

42. Terekhov, A.V., Zatsiorsky, V.M.: Analytical and numerical analysis of inverse optimization problems: conditions of uniqueness and computational methods. Biological Cybernetics **104**(1-2), 75–93 (2011). DOI 10.1007/s00422-011-0421-2

43. Todorov, E.: Optimality principles in sensorimotor control. Nature neuroscience **7**(9), 907–915 (2004). DOI 10.1038/nn1309

44. Todorov, E., Jordan, M.: Smoothness maximization along a predefined path accurately predicts the speed profiles of complex arm movements. Journal of Neurophysiology **80**, 696–714 (1998). URL http://www.ncbi.nlm.nih.gov/pubmed/9705462

45. Uno, Y., Kawato, M., Suzuki, R.: Formation and control of optimal trajectory in human multijoint arm movement. Biological Cybernetics **61**(2), 89–101 (1989). DOI 10.1007/BF00204593

46. Viviani, P., Flash, T.: Minimum-jerk, two-thirds power law, and isochrony: converging approaches to movement planning. Journal of Experimental Psychology: Human Perception and Performance **21**(1), 32–53 (1995). DOI 10.1037/0096-1523.21.1.32

47. Zanchettin, A., Bascetta, L., Rocco, P.: Achieving humanlike motion: Resolving redundancy for anthropomorphic industrial manipulators. Robotics Automation Magazine, IEEE **20**(4), 131–138 (2013). DOI 10.1109/MRA.2013.2283650